


Entanglement transition in the projective transverse field Ising modelNicolai Lang¹* and Hans Peter Büchler¹*Institute for Theoretical Physics III and Center for Integrated Quantum Science and Technology,
University of Stuttgart, 70550 Stuttgart, Germany* (Received 17 June 2020; revised 8 September 2020; accepted 9 September 2020; published 23 September 2020)

Discrete quantum trajectories of systems under random unitary gates and projective measurements have been shown to feature transitions in the entanglement scaling that are not encoded in the density matrix. In this paper, we study the projective transverse field Ising model, a stochastic model with two noncommuting projective measurements and no unitary dynamics. We numerically demonstrate that their competition drives an entanglement transition between two distinct steady states that both exhibit area law entanglement, and introduce a classical but nonlocal model that captures the entanglement dynamics completely. Exploiting a map to bond percolation, we argue that the critical system in one dimension is described by a conformal field theory, and derive the universal scaling of the entanglement entropy and the critical exponent for the scaling of the mutual information of two spins exactly. We conclude with an interpretation of the entanglement transition in the context of quantum error correction.

DOI: [10.1103/PhysRevB.102.094204](https://doi.org/10.1103/PhysRevB.102.094204)**I. INTRODUCTION**

Entanglement has emerged as a powerful tool to characterize states of matter, such as ground states of quantum systems [1], and access their topological properties [2,3], but also to distinguish between generic thermal states and the phenomenon of many-body localization [4]. Recently, a unique transition in random quantum circuits has been identified where the entanglement entropy of the wave function is the key observable that characterizes two different steady states [5–9]. This entanglement transition is driven by the competition between random unitary operations and projective measurements applied at discrete time steps on the wave function. Remarkably, the density matrix of both steady states is maximally mixed, and the transition is only visible in the average of particular properties of wave functions over ensembles of quantum trajectories (see Appendix). In this paper, we study a new type of entanglement transition of quantum circuits that is driven by random projective measurements only.

Quantum circuits are an example of quantum dynamical maps where quantum operations are applied on qubits at discrete time steps. Random unitary operations between neighboring qubits spread entanglement and, if this is the dominating process, entail a volume law for the entanglement entropy [10–12]. (Note that randomness in the unitary dynamics is not necessary to proliferate entanglement and drive entanglement transitions; see, e.g., Refs. [8,13,14].) By contrast, random projective measurements of local observables remove entanglement from the system, and eventually lead to wave functions with area law entanglement. It is the competition between these two processes that gives rise

to the entanglement transition at a finite critical rate of the two processes [5–9]. While the numerical simulation of generic quantum circuits is a computationally hard problem, it was noticed that unitary gates restricted to the Clifford group allow the time evolution of the quantum circuit to be studied numerically even for large systems in the stabilizer formalism [15–18] (the formal statement is referred to as Gottesmann-Knill theorem). This approach allowed for the precise characterization of the critical properties of the entanglement transition [19]. But also analytical methods have been contrived to unravel the nature of the transition [9,20], such as descriptions in terms of conformal field theories [21]. However, it is well established that phase transitions with conventional symmetry breaking, characterized by an order parameter, as well as topological order in nonequilibrium steady states, can appear in driven quantum systems with competing dissipative processes [22,23]. This motivates the question whether entanglement transitions can appear in random quantum circuits with projective measurements only. A necessary ingredient is certainly noncommuting, competing measurements.

In this paper, we present a detailed study of an entanglement transition between two steady states (characterized by quantum jump trajectories of wave functions) that both feature area law entanglement. The quantum circuit is constructed from two noncommuting projective measurements that are applied randomly; this model can be viewed as the natural translation of the transverse field Ising model into a circuit of projective measurements only, and is therefore referred to as the projective transverse field Ising model (PTIM). Also in this particular case, the transition is only visible in the average of certain entanglement measures of wave functions over ensembles of quantum trajectories. While the quantum circuit can be studied numerically using the stabilizer framework, we demonstrate that the entanglement dynamics can be mapped

*nicolai@itp3.uni-stuttgart.de

onto a simpler, classical model which can be simulated more efficiently. In addition, this mapping provides a simple intuition for the spreading of entanglement in our model. We find that the transition exhibits a behavior similar to conventional second-order quantum phase transitions, where at the critical point long-range order is established. Here, the role of long-range order is played by a finite mutual information between two separated spins. Furthermore, the entanglement entropy diverges logarithmically at the transition. These quantities unveil two universal properties of the transition: the prefactor \tilde{c} of the logarithmically diverging entanglement entropy and the critical exponent κ of the algebraic decay of the mutual information. We demonstrate that the critical point is described by bond percolation and determine $\tilde{c} = 3\sqrt{3} \ln(2)/(2\pi)$ and $\kappa = 2/3$ exactly for a one-dimensional setup by mapping to a conformal field theory. Remarkably, the prefactor \tilde{c} is *not* the conformal charge of the underlying conformal field theory, which one would expect for ground states of critical one-dimensional systems [24,25].

The entanglement transition studied in this paper is tightly related to quantum error correction of topologically protected qubits encoded in the ground state of a Majorana chain [26,27]: the two projective measurements can be interpreted as syndrome measurements and local errors, respectively. In this context, the steady state characterized by finite mutual information corresponds to the regime where the quantum information of the code space is preserved. By contrast, in the error-dominated regime the quantum information is lost and the mutual information vanishes. While in the context of (active) quantum error correction it is well established that such phase transitions exist, it is remarkable that an entanglement transition appears even if the syndrome measurements are not recorded and no active error correction takes place. The encoded information is still contained in the wave function of the quantum trajectory but it would require an exponential number of measurements to extract this information. Thus the entanglement transition is in general hidden from our experimental observations.

Finally, we would like to point out that, during finalizing our manuscript, we became aware of recent, closely related studies [28–31] where also purely measurement-driven entanglement transitions between different steady states with area law entanglement were observed. In particular, Ref. [28] studied the critical regime of an equivalent model in one dimension in the Majorana representation; their findings for the critical universal entanglement scaling \tilde{c} agree with ours.

The paper is organized as follows. We introduce the quantum circuit with two noncommuting projective measurements in Sec. II. Although this model can be efficiently simulated as a stabilizer circuit, we present an exact mapping to a simpler, classical model which describes the entanglement dynamics of the system completely. The details of this mapping are presented in Sec. III and the relevant observables are discussed in Sec. IV. In Sec. V we present numerical results: we focus on the one-dimensional chain, demonstrate the divergence of the entanglement entropy at the critical point, and determine the prefactor \tilde{c} of this logarithmic divergence. Then we discuss the mutual information as an indicator of long-range entanglement and show that it exhibits the characteristic behavior of a second-order phase transition. We determine its critical

exponent κ and provide an intuitive interpretation of the transition in terms of Bell clusters. The mapping to percolation is shown in Sec. VI, which allows us to determine the position of the entanglement transition exactly. We conclude this section with a comparison of numerically determined critical points of the entanglement transition for different lattices in two dimensions with known results for bond percolation. In Sec. VII, we exploit the equivalence of our model and bond percolation to determine the conformal field theory that describes the critical point of the one-dimensional system and derive \tilde{c} and κ analytically. We conclude with a discussion of the relation to quantum error correction in Sec. VIII.

II. MODEL

We start with a detailed description of our model. Consider a one-dimensional chain of spin-1/2 degrees of freedom on sites $i \in V_L = \{1, \dots, L\}$. Each spin is represented by Pauli matrices σ_i^α , $\alpha \in \{x, y, z\}$, and the Hilbert space is denoted as $\mathcal{H} = \bigotimes_i \mathbb{C}_i^2$. The quantum circuit is defined by projective measurements of observables O , and the action of such a measurement is denoted as $\mathcal{M}[O]$, i.e.,

$$\mathcal{M}[O](|\Psi\rangle) = \frac{P_\lambda |\Psi\rangle}{\sqrt{\langle \Psi | P_\lambda | \Psi \rangle}} \quad (1)$$

is the new state after measurement of the discrete eigenvalue λ of O with probability $\text{Pr}(\lambda) = \langle \Psi | P_\lambda | \Psi \rangle$; P_λ denotes the projector onto the corresponding eigenspace. Note that $\mathcal{M}[O](|\Psi\rangle)$ is a random variable with values in \mathcal{H} that is parametrized by the input $|\Psi\rangle$; $\mathcal{M}[O](\bullet)$ is not a linear operator (hence the parentheses).

Throughout this paper, we are interested in measurements of the observables σ_i^x and $\sigma_i^z \sigma_{i+1}^z$, i.e.,

$$\mathcal{M}_i^x \equiv \mathcal{M}[\sigma_i^x] \quad \text{with} \quad P_\lambda = \frac{1}{2}(\mathbb{1} + \lambda \sigma_i^x), \quad (2a)$$

$$\mathcal{M}_e^{zz} \equiv \mathcal{M}[\sigma_i^z \sigma_{i+1}^z] \quad \text{with} \quad P_\lambda = \frac{1}{2}(\mathbb{1} + \lambda \sigma_i^z \sigma_{i+1}^z), \quad (2b)$$

for each site i and edge $e = (i, i+1)$ between adjacent sites. The measurement results are $\lambda \in \{-1, +1\}$. It is important to point out that σ_i^x and $\sigma_i^z \sigma_{i+1}^z$ do not commute if they involve the same site so that repeated measurements lead to a nontrivial quantum dynamics.

This quantum dynamics is described as a stochastic process on \mathcal{H} generated by the measurements (2). In contrast to previous studies on entanglement transitions, we do *not* apply additional unitary operations. We start with the initial product state

$$|\Psi(0)\rangle = |++ \dots +\rangle, \quad (3)$$

with $|\pm\rangle = (|0\rangle \pm |1\rangle)/\sqrt{2}$. Then, we evolve the system iteratively as follows (Fig. 1): in each time step, we set the site variable $x_i = 1$ with probability p ($x_i = 0$ otherwise) and— independently— for each edge $e = (i, i+1)$, we set $z_e = 1$ with probability $1 - p$ and again $z_e = 0$ otherwise. The vectors $\mathbf{x} = (x_i)$ and $\mathbf{z} = (z_e)$ determine the sites (edges) on which the observables σ_i^x ($\sigma_i^z \sigma_{i+1}^z$) will be measured. Given the state $|\Psi(t)\rangle$ at time t , the new wave function at $t+1$ is given by (more precisely, drawn from the distribution)

$$|\Psi(t+1)\rangle = \mathcal{M}_{\mathbf{x}}^x \circ \mathcal{M}_{\mathbf{z}}^{zz}(|\Psi(t)\rangle), \quad (4)$$

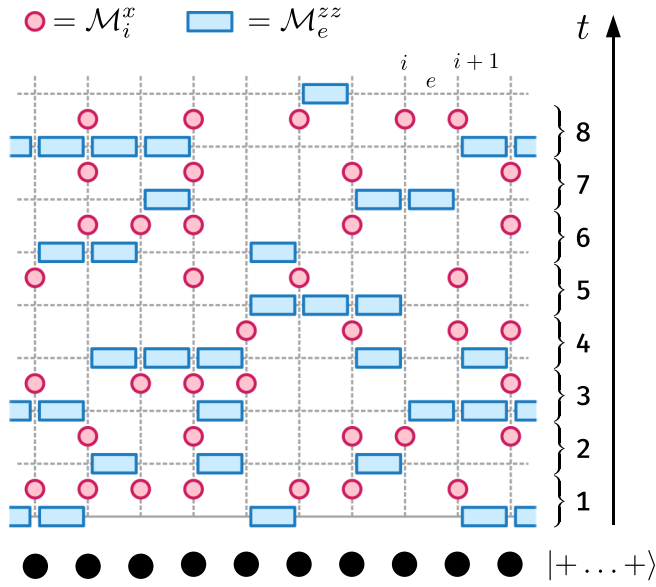


FIG. 1. Projective time evolution. A few typical time steps for $p \approx 0.5$ on a chain of $L = 10$ spins with periodic boundaries. Blue boxes on edges denote measurements \mathcal{M}_e^{zz} on adjacent spins $e = (i, i + 1)$ and red circles measurements \mathcal{M}_i^x on a single spin i . Each time step comprises one row of \mathcal{M}_e^{zz} measurements followed by a row of \mathcal{M}_i^x measurements. Note that the order of \mathcal{M}_e^{zz} measurements does not affect the dynamics as their projectors commute. The system is initialized in the product state $|\dots+\rangle$.

with measurements

$$\mathcal{M}_x = \prod_{i: x_i=1} \mathcal{M}_i^x, \quad \mathcal{M}_z = \prod_{e: z_e=1} \mathcal{M}_e^{zz}. \quad (5)$$

This defines a fully projective time evolution that yields a single quantum trajectory $|\Psi(t)\rangle$ at discrete times $t = 0, 1, 2, \dots$.

We are interested in characteristic properties of such wave functions along a quantum trajectory for a given time t . Denote a generic quantity as $\mathcal{X}(|\Psi(t)\rangle)$ with $\mathcal{X} : \mathcal{H} \rightarrow \mathbb{C}$. Examples are conventional observables such as correlations $\mathcal{X} = \langle \Psi | \sigma_i^z \sigma_j^z | \Psi \rangle$, but also the entanglement entropy $\mathcal{X} = S(A)$ of a subsystem $A \subset V_L$. These quantities are then averaged over many different quantum trajectories, defining the sample averages

$$X \equiv \frac{1}{M} \sum_{|\Psi\rangle \in \mathcal{N}} \mathcal{X}(|\Psi(t)\rangle). \quad (6)$$

Here, $\mathcal{N} = \{|\Psi(\bullet)\rangle\}$ denotes an ensemble of M randomly generated quantum trajectories.

For fixed time t and $M \rightarrow \infty$, the above process defines a classical probability distribution $\mathcal{P}(t)$ on \mathcal{H} . Assuming that there exists a stationary limit, we define the projective transverse field Ising model (PTIM) as being characterized by $\mathcal{P}_\infty = \lim_{t \rightarrow \infty} \mathcal{P}(t)$. Here, we are interested in properties of \mathcal{P}_∞ in dependence of the relative strength of noncommuting measurements $p \in [0, 1]$.

Note that the PTIM has a conserved symmetry: all measurements (2) commute with the symmetry operator $\mathcal{U} = \prod_{i \in V_L} \sigma_i^x$. In particular, the initial state (3) is \mathcal{U} invariant; this property is conserved under the projective dynamics and

restricts the accessible part of the Hilbert space. As a consequence, the density matrix describing the steady state of the PTIM is only maximally mixed up to this symmetry constraint.

III. COLORED CLUSTER MODEL

To study the properties of the PTIM (projective transverse field Ising model), we start with a discussion of the numerical approach that we use to generate samples \mathcal{N} of quantum trajectories $|\Psi(t)\rangle$. It is important to point out that measurements of Pauli operators can be described in the stabilizer formalism [15,16] [this is also true for the initial state (3)]; the projective time evolution of the quantum trajectories can therefore be efficiently simulated on a classical computer—despite the exponentially growing dimension of \mathcal{H} [17,18]. Although simulations in the stabilizer formalism are reasonably efficient, generic, and well understood to bootstrap trustworthy results, it is not the most efficient approach to study the PTIM.

The numerical approach we leverage in this paper is based on an equivalent *classical* process that can be sampled more efficiently. This process turns out to be *nonlocal* and, in addition, provides an intuitive picture of the mechanism that drives the PTIM entanglement transition (see below). The derivation of this process exploits the special structure of the PTIM and is based on the following observations.

(i) Measuring $\sigma_1^z \sigma_2^z$ in the product state (we omit normalizing factors)

$$|++\rangle = |00\rangle + |01\rangle + |10\rangle + |11\rangle \quad (7)$$

yields the entangled Bell pairs $|00\rangle + |11\rangle$ or $|01\rangle + |10\rangle$ with each 50% probability. We refer to both states as a two-qubit Bell cluster (as they are equivalent under local unitary operations, they are identical from an entanglement point of view).

(ii) Measuring $\sigma_2^z \sigma_3^z$ in the product state

$$\begin{aligned} (\alpha|00\rangle + \beta|11\rangle) \otimes |+\rangle \\ = \alpha(|000\rangle + |001\rangle) + \beta(|110\rangle + |111\rangle) \end{aligned} \quad (8)$$

yields the entangled states $\alpha|000\rangle + \beta|111\rangle$ or $\alpha|001\rangle + \beta|110\rangle$ with each 50% probability. The result is therefore an enlarged (three-qubit) Bell cluster. Note that the amplitudes survive.

(iii) Measuring σ_1^x in the three-qubit Bell cluster

$$\begin{aligned} \alpha|000\rangle + \beta|111\rangle \\ = \alpha(|+00\rangle + |-00\rangle) + \beta(|+11\rangle - |-11\rangle) \end{aligned} \quad (9)$$

yields either $|+\rangle \otimes (\alpha|00\rangle + \beta|11\rangle)$ or $|-\rangle \otimes (\alpha|00\rangle - \beta|11\rangle)$ with 50% probability. The result is therefore a shrunken (two-qubit) Bell cluster. Note that again the amplitudes survive (up to a sign that depends on the measurement outcome).

(iv) Measuring $\sigma_2^z \sigma_3^z$ in a state with two two-qubit Bell clusters

$$\begin{aligned} (|00\rangle + |11\rangle) \otimes (\alpha|01\rangle + \beta|10\rangle) \\ = \alpha|0001\rangle + \beta|0010\rangle + \alpha|1101\rangle + \beta|1110\rangle \end{aligned} \quad (10)$$

yields the entangled states $\alpha|0001\rangle + \beta|1110\rangle$ or $\alpha|1101\rangle + \beta|0010\rangle$ with each 50% probability. The result is therefore a merged four-qubit Bell cluster. Again the amplitudes survive.

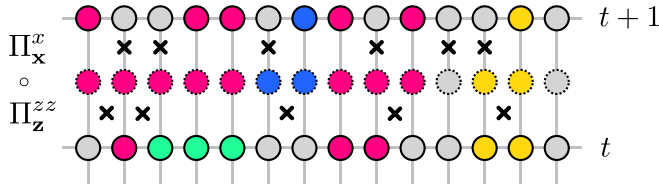


FIG. 2. Colored cluster model. Single time step of the colored cluster model, split into two substeps: (1) the application of Π_z^{zz} on edges (crosses on faces in space-time) that merges/grows/nucleates clusters and (2) Π_x^x on sites (crosses on vertical edges in space-time) that erodes clusters. Sites with dashed boundary represent the intermediate state between t and $t + 1$ and gray sites denote single-site clusters.

We conclude that the dynamics of the PTIM is essentially characterized by the nucleation, growth, decay, and merging of Bell clusters, while phase coherence is preserved. This cluster dynamics does not depend on the specific realization of Bell clusters (i.e., their amplitudes and their spin patterns), for instance,

$$\begin{aligned} &|-000\rangle + |-111\rangle, \\ &|+000\rangle - |+111\rangle, \\ &|-010\rangle + |-101\rangle, \\ &|+011\rangle + |+100\rangle. \end{aligned} \quad (11)$$

All give rise to the same entanglement dynamics and represent the same entanglement structure. This motivates the following classical stochastic process (Fig. 2).

(i) The states of the system are vectors $s \in \mathbb{N}_0^L$, so that the state of each site i is described by a non-negative integer $s_i \in \mathbb{N}_0$; $s_i = 0$ encodes that site i is in a product state and unentangled with the rest of the system. $s_i = n > 0$ marks a site that belongs to a cluster of at least two spins with label n . For example, all four states in (11) can be described collectively by $s = (0, 1, 1, 1)$, where $n = 1$ is the label of the only (three-qubit) Bell cluster.

(ii) The initial state of the process is $s(0) = (0, \dots, 0)$, corresponding to $|\Psi(0)\rangle = |+\dots+\rangle$ in (3) [note that, e.g., $|\Psi(0)\rangle = |-\dots-\dots+\rangle$ would not alter the entanglement dynamics and therefore corresponds to the same state $s(0)$].

(iii) Instead of measurements, the transformation

$$s(t+1) = \Pi_x^x \circ \Pi_z^{zz}(s(t)) \quad (12)$$

is applied iteratively with

$$\Pi_x^x = \prod_{i: x_i=1} \Pi_i^x, \quad \Pi_z^{zz} = \prod_{e: z_e=1} \Pi_e^{zz}. \quad (13)$$

The function Π_i^x acts locally and is defined by $s' = \Pi_i^x(s)$ with $s'_j = s_j$ for all $j \neq i$ and $s'_i = 0$. By contrast, the function Π_e^{zz} for $e = (i, j)$ acts *nonlocally* and is defined via $s' = \Pi_e^{zz}(s)$ as follows (sites that are not mentioned remain unchanged).

Case 1: $s_i = 0$ and $s_j = 0$; then $s'_i := \text{next}(s) =: s'_j$. Here, $\text{next}(s) = \min(n \in \mathbb{N} \setminus s)$ returns the smallest integer that is not used as a cluster label in s . This process creates a new, independent cluster with two spins.

Case 2a: $s_i \neq 0$ and $s_j = 0$; then $s'_j := s_i$. This process joins site j to the cluster of site i .

Case 2b: $s_i = 0$ and $s_j \neq 0$; then $s'_i := s_j$. This process joins site i to the cluster of site j .

Case 3: $s_i \neq 0$ and $s_j \neq 0$. Let $s = \min(s_i, s_j)$; then set $s_l := s$ for all sites l with $s_l = s_i$ or $s_l = s_j$. This process merges two clusters and thereby reduces the number of independent clusters by one without reducing the number of spins that belong to clusters.

The last case defines a nonlocal transformation—a consequence of the quantumness of the PTIM where the nonlocality of clusters is naturally realized by entanglement.

Note that one can interpret the PTIM as a local quantum simulator for this nonlocal classical process. In the following, we color the sites i according to their state s_i and refer to this model as the colored cluster model (CCM). It is this simpler but equivalent model that we evolve and sample numerically. We also cross-checked our results numerically for the PTIM using the stabilizer formalism [15–18].

IV. ENTANGLEMENT MEASURES

By simulating the CCM (colored cluster model), we lose access to some properties of the PTIM. In particular, conventional expectation values of the wave function along the quantum trajectory are no longer accessible. However, the entanglement transition cannot be detected by observables anyway as the density matrix in the steady state is maximally mixed (up to symmetry constraints). Indeed, the appropriate quantities that characterize the entanglement transition are the entanglement entropy and the mutual information—both of which can be efficiently computed using the CCM.

The entanglement entropy of a subsystem $A \subset V_L$ for a wave function along a quantum trajectory is defined as

$$S(A) \equiv -\text{Tr}[\rho_A \log_2 \rho_A], \quad (14)$$

with $\rho_A = \text{Tr}_{V_L \setminus A}[\rho]$ the reduced density matrix of the subsystem. In terms of Bell clusters, $S(A)$ counts the number of clusters with support both in A and $\bar{A} \equiv V_L \setminus A$, a quantity that can be easily computed from CCM states $s(t)$. Note that here we define the entanglement entropy with the binary logarithm \log_2 such that each Bell cluster contributes 1 instead of $\ln 2$.

The actual quantity of interest is the entanglement entropy $S(A)$ averaged over many, randomly sampled quantum trajectories. Therefore, we denote by $\bar{S}(A)$ the sample-averaged entanglement entropy as defined in (6). We also define $S_L(l)$ as the (sample-averaged) entanglement entropy of l contiguous spins in the center of a chain with L sites, i.e., A comprises the l sites in the interval $[L/2 - l/2, \dots, L/2 + l/2]$.

Now consider two disjoint subsystems $A, B \subset V_L$. The mutual information $I(A, B)$ between A and B is defined as

$$I(A, B) \equiv S(A) + S(B) - S(A \cup B). \quad (15)$$

A nonvanishing value of $I(A, B)$ indicates entanglement between the subsystems A and B for wave functions along a quantum trajectory [32,33]. Here we are mainly interested in the mutual information between two spins at sites $i, j \in V_L$, that is

$$I(i, j) \equiv S(\{i\}) + S(\{j\}) - S(\{i, j\}). \quad (16)$$

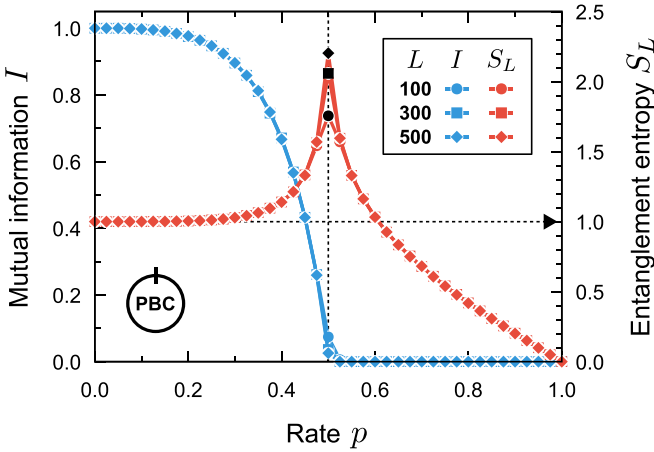


FIG. 3. Entanglement transition. Numerical results for the entanglement entropy $S_L(L/2)$ (red) and the mutual information $I(1, 1 + L/2)$ (blue) as functions of the rate p for systems of length $L = 100, 300, 500$ (circles, squares, diamonds) with periodic boundary conditions (PBC). At the critical point $p = 0.5 = p_c$, the entanglement entropy grows logarithmically with the system size (black markers). Each point is based on 10^5 sampled trajectories.

For a state $|\Psi\rangle$ along a quantum trajectory of the PTIM, $I(i, j)$ is an $L \times L$ matrix that encodes the structure of Bell clusters in the system completely. For example, $|\Psi\rangle = |0, 0, 0, 0\rangle_{1234}$ but also $|\Psi\rangle = (|0, 0\rangle + |1, 1\rangle)_{12} \otimes (|0, 1\rangle + |1, 0\rangle)_{34}$ yields $I(1, 4) = 0$, since spins 1 and 4 are not part of a common Bell cluster. By contrast, $|\Psi\rangle = (|0, 0\rangle + |1, 1\rangle)_{14} \otimes (|0, 1\rangle + |1, 0\rangle)_{23}$ yields $I(1, 4) = 2$ and for $|\Psi\rangle = |0, 0, 0, 0\rangle_{1234} + |1, 1, 1, 1\rangle_{1234}$ we have $I(1, 4) = 1$; in both cases, spins 1 and 4 belong to the same Bell cluster. If we consider $I(i, j)$ as the adjacency matrix of a graph, the connected components of this graph are in one-to-one correspondence with the Bell clusters of $|\Psi\rangle$. In the language of the CCM, it is $I(i, j) = 0$ for sites of different color $s_i \neq s_j$ (or $s_i = 0 = s_j$) and $I(i, j) = 1$ for sites of the same color $s_i = s_j \neq 0$; for clusters that contain only the two sites i and j , it is $I(i, j) = 2$.

V. NUMERICAL RESULTS

For the following results, we sampled typically $M \sim 10^5 - 10^7$ trajectories for sufficiently long time $t \sim 2 \times 10^3$ such that all quantities of interest reached their equilibrium values in the steady state. The quantities of interest are the sample-averaged entanglement entropy $S_L(l)$ and the mutual information $I(i, j)$.

A. Entanglement entropy

In Fig. 3 we show the entanglement entropy $S_L(L/2)$ as a function of p for chains of lengths $L = 100, 300, 500$ with periodic boundaries. For $p \rightarrow 0$ (only \mathcal{M}_e^{zz}), the entanglement entropy saturates at 1 since the system approaches a global Bell cluster $|\mathbf{m}\rangle + |\bar{\mathbf{m}}\rangle$ where $|\bar{\mathbf{m}}\rangle \equiv \mathcal{U}|\mathbf{m}\rangle$ with $\mathbf{m} \in \mathbb{Z}_2^L$ a random spin pattern in the z basis; here again $\mathcal{U} = \prod_i \sigma_i^x$ denotes the global symmetry which is conserved along the quantum trajectory. For $p \rightarrow 1$ (only \mathcal{M}_i^x), the system approaches the unentangled product state $|+\dots+\rangle$ so that $S_L(L/2)$ vanishes smoothly. For $0 < p < 1$ there seems to be a slow

divergence at the critical value $p_c \approx 0.5$ that leads to a weakly nonanalytic behavior of $S_L(L/2)$ for $L \rightarrow \infty$. Below, we will demonstrate analytically that the transition indeed takes place at the critical point $p_c = 0.5$. The two regimes can be understood intuitively in the context of Bell clusters if we recall that $S_L(L/2)$ counts the number of independent Bell clusters with support in both halves of the system.

(i) For $p \gg p_c$, the projections onto $|\pm\rangle$ dominate and make the clusters decay rapidly; they cannot grow to extensive size and cross the two boundaries of the subsystem rarely.

(ii) For $p \approx p_c$, nucleation and growth of clusters on one side and annihilation and decay on the other side are balanced. Clusters become deconfined and spread throughout the system. Typically, two independent clusters connect the two halves of the system: one located at each of the two boundaries of the subsystem. In rare cases, additional, independent clusters contribute entanglement, so that $S_L(L/2) \gtrsim 2$ for long chains.

(iii) For $p \ll p_c$, the growth of clusters dominates. Since the probability that two independent clusters merge grows exponentially with their surface, the probability for two or more extensive clusters vanishes exponentially. This is a condensation mechanism where newly created clusters (“condensation nuclei”) quickly get absorbed by the macroscopic cluster (the “condensate”). This explains why $S_L(L/2) \rightarrow 1$ quickly saturates.

Thus the average lifetime of newly spawned clusters vanishes quickly for both $p \rightarrow 1$ and $p \rightarrow 0$. For $p \rightarrow 1$, this is due to the destructive force of the \mathcal{M}_i^x measurements that dissolve the clusters. For $p \rightarrow 0$, the clusters do not dissolve but get absorbed by the condensate and this mechanism becomes more efficient when the density of the condensate increases.

In Fig. 4(a) we show the behavior of $S_L(l)$ for $0 \leq l \leq L$ for different parameters p . As expected, we observe that for $p \neq p_c$ the entanglement entropy saturates quickly, indicating area law entanglement. However, this behavior is modified at the critical point by a logarithmic contribution. The slow divergence of $S_L(l)$ at criticality for $L \rightarrow \infty$ with $l/L = \text{const}$ (recall Fig. 3), and for $l \rightarrow \infty$ with $l \ll L$ is a well-known feature of critical systems in one dimension that can be described by a conformal field theory: the scaling law for ground states of conformally invariant systems with periodic boundaries at the critical point is asymptotically described by [24,25]

$$S_L(l) \sim \frac{c}{3} \log_2 \left[\frac{L}{\pi} \sin \left(\pi \frac{l}{L} \right) \right] \stackrel{l \ll L}{\approx} \frac{c}{3} \log_2(l), \quad (17)$$

with the central charge c (up to a nonuniversal constant).

In the following, we analyze whether the critical entanglement scaling of the PTIM exhibits the same behavior. To this end, we consider the normalized entanglement entropy

$$\Delta S(l/L) \equiv S_L(l) - S_L(L/2) \sim \frac{\tilde{c}}{3} \log_2 \left[\sin \left(\pi \frac{l}{L} \right) \right] \quad (18)$$

that is expected to be independent of the system size L . In Fig. 5 we plot this quantity for system sizes $L = 100, \dots, 300$ at criticality. The collapse of data for different L is remarkable and, fitting Eq. (18) to our numerical data, we find the prefactor $\tilde{c} \approx 0.57$. This observation suggests that the critical properties of the PTIM are described by a conformal field

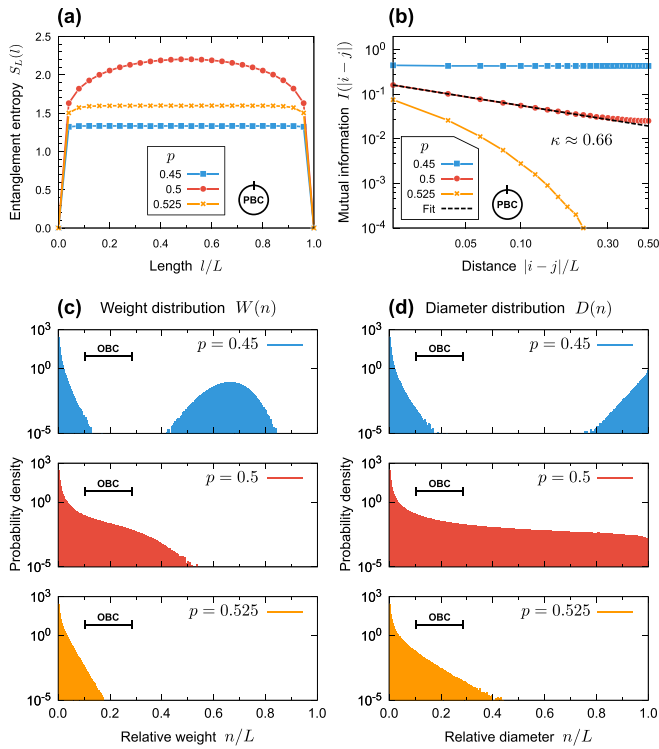


FIG. 4. Entanglement structure. Various quantities characterizing the entanglement structure of a chain with length $L = 500$ above, at, and below the critical point; all results are based on 10^6 sampled trajectories: (a) entanglement entropy $S_L(l)$ as a function of the length l/L of the subsystem for a chain with periodic boundary conditions. The system obeys an area law in both phases, $p = 0.45 < p_c$ and $p = 0.525 > p_c$, with a logarithmic contribution at the critical point $p = 0.5 = p_c$. (b) Mutual information $I(i, j) = I(|i - j|)$ as a function of the distance $|i - j|/L$ for a chain with periodic boundary conditions. $I(|i - j|)$ vanishes exponentially for $p > p_c$ and saturates at a finite value for $p < p_c$. At the critical point $p = p_c$, it is well described by the algebraic decay $I(|i - j|) = \alpha |i - j|^{-\kappa}$ with fitted exponent $\kappa \approx 0.66$ and nonuniversal fit parameter α (dashed black line). (c) Probability density $W(n) \times L$ of the relative weight n/L of Bell clusters for a chain with open boundary conditions. At the entanglement transition, clusters of extensive weight emerge. (d) Probability density $D(n) \times L$ of the relative diameter n/L of Bell clusters for a chain with open boundary conditions. At the entanglement transition, clusters with diameters on all length scales exist.

theory. Indeed, we will argue below that the critical properties are determined by a conformal field theory with central charge $c = 0$, while the prefactor of the entanglement entropy takes the exact value $\tilde{c} = 3\sqrt{3} \ln(2)/(2\pi) \approx 0.573$. In contrast to ground states of critical one-dimensional quantum systems, the prefactor of the entanglement entropy is not the central charge.

B. Mutual information

Next, we analyze the sample-averaged mutual information $I(i, j)$ in the steady state. A finite value indicates a finite probability to find a Bell cluster that encompasses sites i and j . In Fig. 3, the mutual information $I = I(1, 1 + L/2)$ as a function

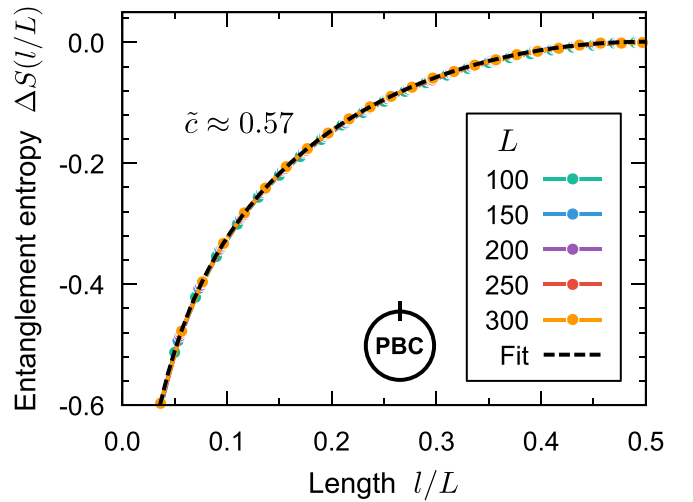


FIG. 5. Critical scaling. Entanglement entropy $\Delta S(l/L)$ as a function of the subsystem size l/L for chains of different length L with periodic boundary conditions at the critical point $p = 0.5 = p_c$. The data collapse is almost perfect and the prediction for critical systems of the form $\Delta S(l/L) = \tilde{c}/3 \log_2 \xi(l/L)$ with $\xi(x) = \sin(\pi x)$ describes the dependency remarkably well for the fit parameter $\tilde{c} \approx 0.57$ (dashed black line). Each curve is based on 10^6 sampled trajectories.

of p for a chain with periodic boundaries is shown. Clearly the system undergoes a continuous entanglement transition at the critical value $p_c \approx 0.5$, where $I > 0$ for $p < p_c$ and $I = 0$ for $p > p_c$. This is consistent with our interpretation above: below the critical value, there is a “condensate” of Bell clusters, that is, a single, macroscopic cluster that permeates the whole system, creating entanglement between spins that are far apart. The limit $I_\infty = \lim_{|i-j| \rightarrow \infty} I(i, j)$ is a measure for the density of the macroscopic cluster and continuously converges to 1 for $p \rightarrow 0$. This behavior is in close analogy to a conventional second-order quantum phase transition where, at the critical point, long-range order is established. Similarly, at the entanglement transition, the mutual information for distant spins attains a finite value.

In Fig. 4(b) we show the behavior of $I(i, j)$ for increasing distance between the two spins [note that $I(i, j) = I(|i - j|)$ because of translation invariance]. While for $p > p_c$ the mutual information $I(i, j)$ vanishes exponentially with the distance, it saturates at a finite value for $p < p_c$. However, at the critical point p_c , it exhibits an algebraic decay with critical exponent κ ,

$$I(i, j) = I(|i - j|) \sim \frac{\alpha}{|i - j|^\kappa}, \quad (19)$$

with nonuniversal parameter α . From the numerical results, we find the critical exponent $\kappa \approx 0.66$. Below, we determine this critical exponent by arguments based on the mapping of the critical regime to a conformal field theory and find the exact value $\kappa = 2/3$.

C. Distribution of Bell clusters

To quantify the emergence of a macroscopic cluster at the entanglement transition, we define the *diameter* $d(B)$ of a Bell

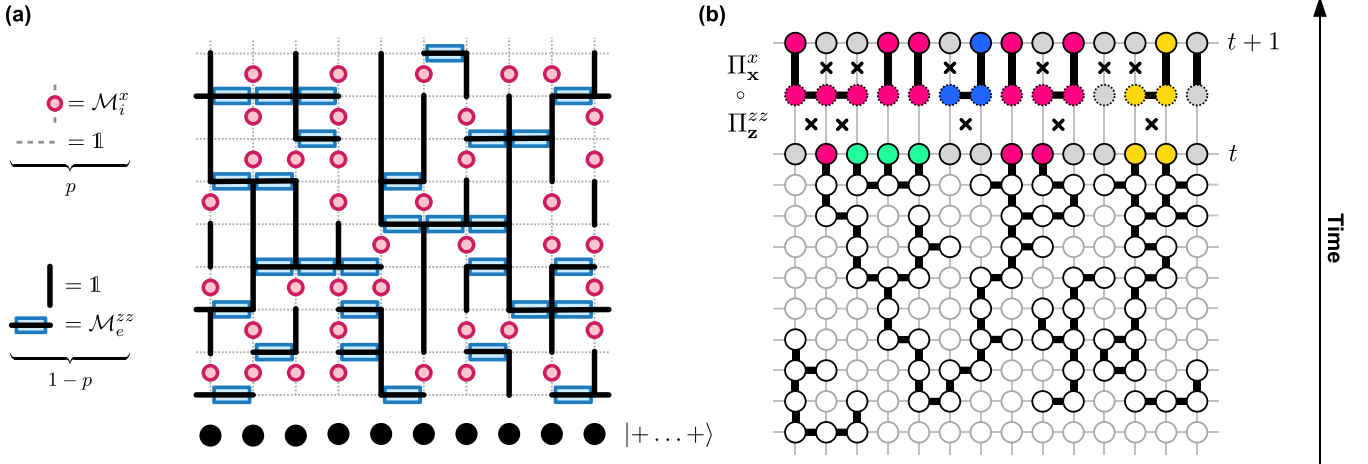


FIG. 6. Percolation. (a) The same measurement pattern as in Fig. 1. Here we mark horizontal edges with \mathcal{M}_e^{zz} measurements and vertical edges *without* \mathcal{M}_i^x measurements as active (bold black lines). Then, the probability for both horizontal and vertical edges to be active is $1 - p$ and the projective dynamics gives rise to isotropic bond percolation on a square lattice in space-time. (b) A possible history for the CCM state in Fig. 2. Sites at time t have the same color if and only if they are connected via active edges in space-time.

cluster $B \subset V_L$ as

$$d(B) = \max\{|i - j| \mid i, j \in B\} \quad (20)$$

for systems with *open* boundaries; this is just $|i_{\leftarrow} - i_{\rightarrow}|$ with the leftmost (rightmost) spin i_{\leftarrow} (i_{\rightarrow}) that belongs to B . In addition, we define the *weight* $|B|$ as the number of spins that make up the cluster B . Let \mathcal{B}_Ψ denote the set of all Bell clusters of a given wave function $|\Psi\rangle$ along a quantum trajectory (we count single spins as one-qubit Bell clusters). The distribution $\mathcal{D}(n)$ with $n = 0, 1, \dots, L - 1$ for this wave function is defined as

$$\mathcal{D}(n) = |\{B \in \mathcal{B}_\Psi \mid d(B) = n\}| / |\mathcal{B}_\Psi|, \quad (21)$$

and similarly for the weight

$$\mathcal{W}(n) = |\{B \in \mathcal{B}_\Psi \mid |B| = n\}| / |\mathcal{B}_\Psi|. \quad (22)$$

In Fig. 4(d), we show the diameter distribution $\mathcal{D}(n)$, i.e., the average over quantum trajectories of the distribution $\mathcal{D}(n)$, as a function of the relative diameter n/L . In Fig. 4(c), we show the averaged distribution $\mathcal{W}(n)$ as a function of the relative weight n/L . Note that, at the entanglement transition, the distribution $\mathcal{D}(n)$ features a long tail (demonstrating the existence of clusters on all length scales), while for $p < p_c$ it becomes bimodal with considerable contributions for diameters $n \sim L$, indicating the emergence of clusters that permeate the system. By contrast, the weight distribution $\mathcal{W}(n)$ evolves towards a saddle point at p_c , which then leads to a second maximum at weights $n \sim L/2$ that shifts continuously to $n \sim L$ for $p \rightarrow 0$. These observations illustrate that the extensive cluster is sparse close to the critical point and grows in density for $p \rightarrow 0$, where more and more spins “condense” into the macroscopic Bell cluster.

To conclude the discussion of numerical results, we point out that the presence of a finite density of z -polarized spins $|\dots \uparrow \dots \downarrow \dots\rangle$ in the initial state (3) (“ z poisoning”) alters the entanglement dynamics dramatically. In particular, for $p \rightarrow 0$ both entanglement entropy and mutual information vanish smoothly as no global Bell cluster can be established. Indeed, while there is no process that can *collapse*

Bell clusters for purely x -polarized initial states, z -polarized spins trigger an avalanche of cluster collapses by \mathcal{M}_e^{zz} measurements that (for small p) quickly drive the system into a product state. Interestingly, even with z poisoning, there are still critical fluctuations at p_c as indicated by a sharp peak of the entanglement entropy. We do not consider effects of z poisoning in this paper.

VI. PERCOLATION

The PTIM and the CCM (which captures the entanglement properties of the PTIM) are intimately linked to bond percolation. The mapping is illustrated in Fig. 6(a) and described in the following. The discrete time steps give rise to a square lattice in space-time where each time step comprises one horizontal row of edges and all vertical edges that connect it to the next row. If we mark horizontal edges with $z_e = 1$ and vertical edges with $x_i = 0$ as “active” (bold black edges), the probability for activity is in both cases $1 - p$. Thus every sequence of measurements on the spins on a one-dimensional PTIM is in one-to-one correspondence with a pattern of active bonds on its space-time square lattice. Following our observations that led to the construction of the CCM, it is easy to see that, at a given time t , two spins i and j are entangled (belong to the same Bell cluster; in the CCM: have the same color) if and only if the two sites are connected by a path of active edges on the space-time lattice in the past; see Fig. 6(b). This observation immediately implies that the critical point for the entanglement transition of the PTIM coincides with the transition for bond percolation; on a square lattice, this transition takes place at $p_c = 0.5$ (which follows exactly from duality arguments [34]). This is in agreement with the numerical results above.

This close relation between bond percolation and the PTIM allows us immediately to determine also the critical point of the entanglement transition in higher dimensions. It is straightforward to define the PTIM on arbitrary lattices \mathcal{L} where the measurements \mathcal{M}_i^x act with probability p on vertices $i \in V(\mathcal{L})$ and the measurements \mathcal{M}_e^{zz} with probability

TABLE I. Critical values. Estimates of critical values p_c for various lattices. In 2D, we compare them with numerical values \tilde{p}_c from Ref. [35] for three-dimensional bond percolation on stacks of the corresponding 2D lattices. Values marked with an asterisk are exact. Our estimates are based on lattices up to 50×50 spins.

Dimension	Lattice	p_c	\tilde{p}_c	Percolation lattice
1		0.5	0.5*	Square
2	Square	0.75	0.7512	Cubic
2	Kagome	0.74	0.7437	Stacked Kagome
2	Honeycomb	0.70	0.6907	Stacked honeycomb
2	Triangular	0.83	0.8140	Stacked triangular

$1 - p$ on edges $e \in E(\mathcal{L})$. The corresponding CCM is then induced by bond percolation on the half-infinite stack of lattices \mathcal{L} with vertical edges connecting vertices of adjacent layers (for instance, the PTIM on the two-dimensional square lattice is described by bond percolation on the (2+1)-dimensional cubic lattice). We estimated the critical values p_c for square, Kagome, honeycomb, and triangular lattice from simulations with up to 50×50 spins. In Table I we compare these values with known (numerical) results for the corresponding bond percolation problems in three dimensions [35] and find reasonable agreement between them.

Furthermore, we would like to briefly comment on the more generic case where \mathcal{M}_i^x and \mathcal{M}_e^{zz} occur with independent probabilities p^x and p^z , respectively. Then the connectivity on the space-time lattice is determined by *anisotropic* bond percolation [36] with probability $p_\perp = p^z$ for horizontal edges and $p_\parallel = 1 - p^x$ for vertical edges. In two dimensions it can be shown by duality arguments that the system is critical for $p_\perp + p_\parallel = 1$, or, equivalently, $p^x = p^z$ [34]. If we choose the parametrization $p^z = q$ and $p^x = rq$, the entanglement transition occurs for $r_c = 1$ and is independent of q (which quantifies the overall measurement rate). We verified this numerically and found no dependence of the entanglement transition of the PTIM in one dimension on the measurement rate q . However, in higher dimensions, the relation between the critical values $p_{\perp,c}$ and $p_{\parallel,c}$ is no longer linear [36]. As a consequence, we expect the critical ratio $r_c = p^x/p^z$ for the PTIM on the square lattice to depend on the measurement rate q . We checked this numerically and indeed found a shift towards larger ratios r_c in the limit $q \rightarrow 0$.

Finally, we point out that in the limit $q \rightarrow 0$ measurements become rare events in each time step so that the dynamics can be approximated by independent Poisson processes on all sites and edges for \mathcal{M}_i^x and \mathcal{M}_e^{zz} measurements with rate parameters $\lambda^x/\lambda^z = r$. Then, the order of measurements becomes irrelevant—in contrast to the PTIM where in each time step we first apply \mathcal{M}_e^{zz} and subsequently \mathcal{M}_i^x ; cf. Eq. (4). In this limit, the process belongs to the family of continuum random cluster models [37–40] in $d + 1$ dimensions which are known to describe quantum Q -state Potts models [39–41] in d dimensions. In particular, percolation is described by the $Q \rightarrow 1$ limit of the Potts model, which is an important observation for the derivation of the correct conformal field theory at the critical point of the (1+1)-dimensional PTIM.

VII. CONFORMAL FIELD THEORY AT THE CRITICAL POINT

The close relation between the PTIM in one dimension and bond percolation on a two-dimensional square lattice allows us to derive the conformal field theory describing the critical point of the entanglement transition. First, note that bond percolation on the square lattice is the simplest random cluster model with cluster weight $Q = 1$ (more generally, cluster models are equivalent to classical Q -state Potts models [38]). Planar random cluster models can be mapped to six-vertex models [42] which, at the critical point, have an equivalent description as a dense gas of oriented loops with weight \sqrt{Q} [43]. Interpreting the oriented loops as contour lines of a discrete “height” field $\phi(\mathbf{x}) \in \pi\mathbb{Z}$ establishes an equivalent description in terms of a solid-on-solid (SOS) model [44,45]. At large distances and after coarse graining, the height field can be approximated by a continuous field $\Phi(\mathbf{x}) \in \mathbb{R}$ and the solid-on-solid model renormalizes to a Gaussian fixed point with coupling $g = 1 - e_0$ where $\sqrt{Q} = 2 \cos(\pi e_0)$ [46–48]. If defined on a cylinder (corresponding to a periodic PTIM in one dimension), the correct weighting of noncontractible loops makes it necessary to put charges $\pm e_0$ on the two boundaries of the cylinder [42,48,49] by inserting vertex operators $V_\pm^0 = \exp(\pm i e_0 \Phi)$. This modifies the vacuum energy on the cylinder and shifts the central charge to $c = 1 - 6e_0^2/(1 - e_0)$ [48]. For percolation, we have $e_0 = 1/3$ and the central charge vanishes, i.e., $c = 0$; therefore, the prefactor \tilde{c} for the entanglement entropy (18) must play another role.

In the following, we derive the prefactor \tilde{c} for the asymptotic behavior of the entanglement entropy in the conformal field theory. The approach is motivated by recent results on the valence bond entanglement entropy in the ground state of an antiferromagnetic spin chain [50]. We start by considering a half-infinite cylinder by shifting the lower boundary to infinity. Such a half-infinite cylinder is conveniently mapped to the complex plane, which leaves us with a disk where V_-^0 is inserted at the origin and V_+^0 somewhere on the boundary. We follow now the lines of Ref. [50] and split V_\pm^0 into two vertex operators $V_\pm^e = \exp[i(\pm e + e_0/2)\Phi]$ with scaling dimension

$$h = \frac{e^2 - (e_0/2)^2}{1 - e_0} \quad (23)$$

and $e \in \mathbb{R}$ a free parameter; see Fig. 7(a). The pair of vertex operators V_\pm^e , inserted at x_1 and x_2 on the boundary, modifies the weight of loops that connect the boundary segment $A = [x_1, x_2]$ of length $\Delta x = |x_1 - x_2|$ with the rest of the boundary \bar{A} . Therefore, the correlation function of the vertex operators can be written as

$$\mathcal{V}_A(w) = \langle V_+^e(x_1) V_-^e(x_2) \rangle = \frac{\sum \tilde{w}^{\tilde{N}} w^{N_A}}{\sum \tilde{w}^{\tilde{N} + N_A}} \sim \frac{1}{\Delta x^{2h}}, \quad (24)$$

where the sums go over all allowed loop configurations. N_A is the number of loops connecting A and \bar{A} , whereas \tilde{N} counts the loops attached with both ends either to A or to \bar{A} . The weights are $\tilde{w} = 2 \cos(\pi e_0/2)$ and $w = 2 \cos(\pi e)$.

Relation (24) allows us to derive the entanglement entropy $S(A)$ of segment A ; see Fig. 7(a). Each independent Bell cluster of the PTIM that lives both in A and \bar{A} increases $S(A)$ by one. In the picture of discrete bond percolation, such Bell

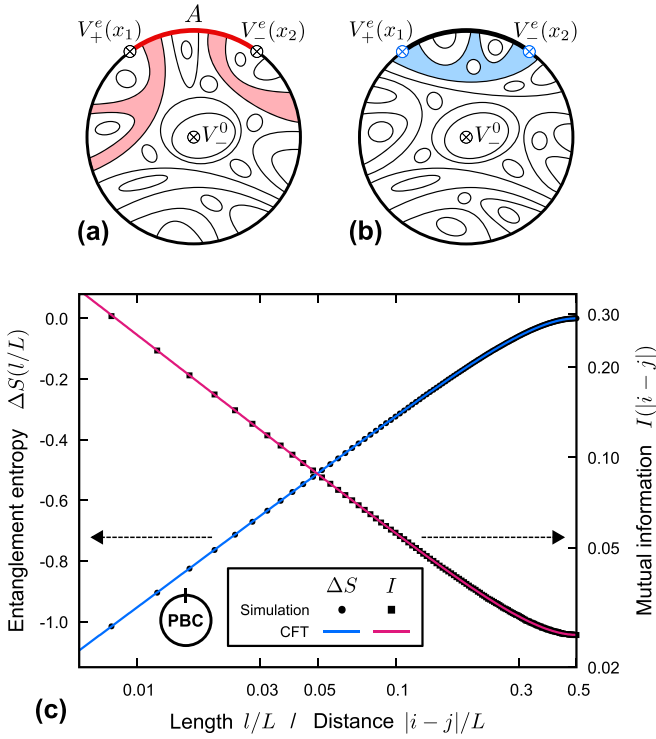


FIG. 7. Conformal field theory. (a),(b) Field configurations on the half-infinite cylinder mapped to the complex plane. Vertex operator insertions are indicated by \otimes . (a) Scaling of the entanglement entropy $S(A)$. Field configurations with contours that connect A (red segment) with the environment (black boundary) contribute to the entanglement between them (light red domains). (b) Scaling of the mutual information $I(x_1, x_2)$. Field configurations that connect the points x_1 and x_2 (light blue domain) contribute to the mutual information between them. (c) Comparison of numerical results (squares and bullets) and theoretical predictions (solid lines) for the PTIM at criticality. The simulations are based on 10^7 trajectories for a system of length $L = 500$ with periodic boundary conditions. The CFT predictions are of the form $\Delta S(l/L) = \tilde{c}/3 \log_2 \xi(l/L) + \alpha$ and $I(i, j) = I(|i - j|) = \beta \xi^{-\kappa}(|i - j|) + \gamma$ with \tilde{c} and κ as given in the text and α, β, γ nonuniversal fit parameters; $\xi(x) = \sin(\pi x)$ accounts for the finite size and the periodic boundaries. Note that the plot for ΔS is logarithmic on the l/L axis; the plot for I is logarithmic on both axes.

clusters derive from clusters of edges in space-time that connect A with \bar{A} . Since the loops of the continuum model essentially describe the *boundaries* of these clusters, we conclude that $S(A) \sim \langle N_A \rangle / 2$. The average number of loops $\langle N_A \rangle$ derives from (24) by the relation $\langle N_A \rangle = \tilde{w} [\partial_w \mathcal{V}_A(w)]_{w=\tilde{w}}$. Given the scaling dimension h (23) for the vertex operators, we find the logarithmic divergence of the entanglement entropy

$$S(A) \sim \frac{\langle N_A \rangle}{2} \sim \frac{\sqrt{3} \ln 2}{2\pi} \log_2 \Delta x. \quad (25)$$

A comparison with Eq. (17) implies the exact value of the prefactor for the entanglement entropy at the critical point

$$\tilde{c} = \frac{3\sqrt{3} \ln 2}{2\pi}. \quad (26)$$

It matches the numerical results in Fig. 7(c) remarkably well. This scaling has also been found in the Majorana representation of Ref. [28].

Next, we focus on the mutual information $I(x_1, x_2)$ between the two boundary points x_1 and x_2 of A ; see Fig. 7(b). For $I(x_1, x_2) = 1$, a percolation cluster that connects the sites x_1 and x_2 is required. This precludes clusters connecting the interior of A with the interior of \bar{A} . We therefore argue that $I(x_1, x_2) \sim \langle \delta_{N_A=0} \rangle$. Note that we expect $I(x_1, x_2) = 2$ (indicating monogamous entanglement between the two sites) to be irrelevant in the continuum limit. Using (24), we find $\langle \delta_{N_A=0} \rangle = \mathcal{V}_A(w \rightarrow 0)$. To set $w = 2 \cos(\pi e) = 0$, we choose $e = 1/2$ and find with (23) the scaling dimension $h = 1/3$ of the vertex operators. Consequently,

$$I(x_1, x_2) \sim \langle \delta_{N_A=0} \rangle \sim \frac{1}{(\Delta x)^\kappa}, \quad (27)$$

with $\kappa = 2h = 2/3$, again consistent with numerical results to a remarkable degree; see Fig. 7(c).

VIII. RELATION TO QUANTUM ERROR CORRECTION

Here we reinterpret the PTIM dynamics as a competition between projective errors and syndrome measurements on a topological quantum memory—an approach also successfully applied for the entanglement transition in the unitary regime [51–53]. To this end, consider an open chain of L spinless fermions c_i and define the Majorana modes

$$\gamma_{2i-1} = c_i + c_i^\dagger, \quad \gamma_{2i} = i(c_i - c_i^\dagger), \quad (28)$$

with $\{\gamma_i, \gamma_j\} = 2\delta_{ij}$, $\gamma_i^\dagger = \gamma_i$, and $\gamma_i^2 = 1$. Define stabilizer operators $S_{e=(i,i+1)} = i\gamma_{2i}\gamma_{2i+1}$ for $i = 1, \dots, L-1$, which obey $S_e^\dagger = S_e$, $S_e^2 = 1$, and $[S_e, S_{e'}] = 0$. We are interested in the twofold degenerate ground state space of the quadratic fermion Hamiltonian [26]

$$H = - \sum_e S_e = - \sum_{i=1}^{L-1} i\gamma_{2i}\gamma_{2i+1} \quad (29)$$

characterized by $S_e = 1$ on all edges e . Let $\{|g_0\rangle, |g_1\rangle\}$ be a basis of the ground state space, the *code space* of the Majorana chain quantum code [27]. A logical qubit with amplitudes α and β is then encoded as $|\Phi\rangle = \alpha|g_0\rangle + \beta|g_1\rangle$.

The elementary errors of the code are generated by the Hermitian on-site operators $E_i = i\gamma_{2i-1}\gamma_{2i}$ and, due to $S_e E_i = -E_i S_e$ for $i \in e$, lead to excitations of the Hamiltonian (29). In the following, we assume that the environment measures E_i projectively with probability p per site and time step. To detect and correct these errors, we are allowed to measure the stabilizers S_e projectively and use the measurement outcomes, the so called error syndrome. Common schemes to protect the qubit $|\Phi\rangle$ from decoherence employ time-periodic measurements of all stabilizers and then use majority voting on the syndromes to decide on unitary corrections in each time step [27,54]. Here we modify this scheme and perform stabilizer measurements *randomly* with probability $1 - p$ per edge and time step. This can be interpreted as a faulty implementation of the code where syndrome measurements fail to be executed with probability p .

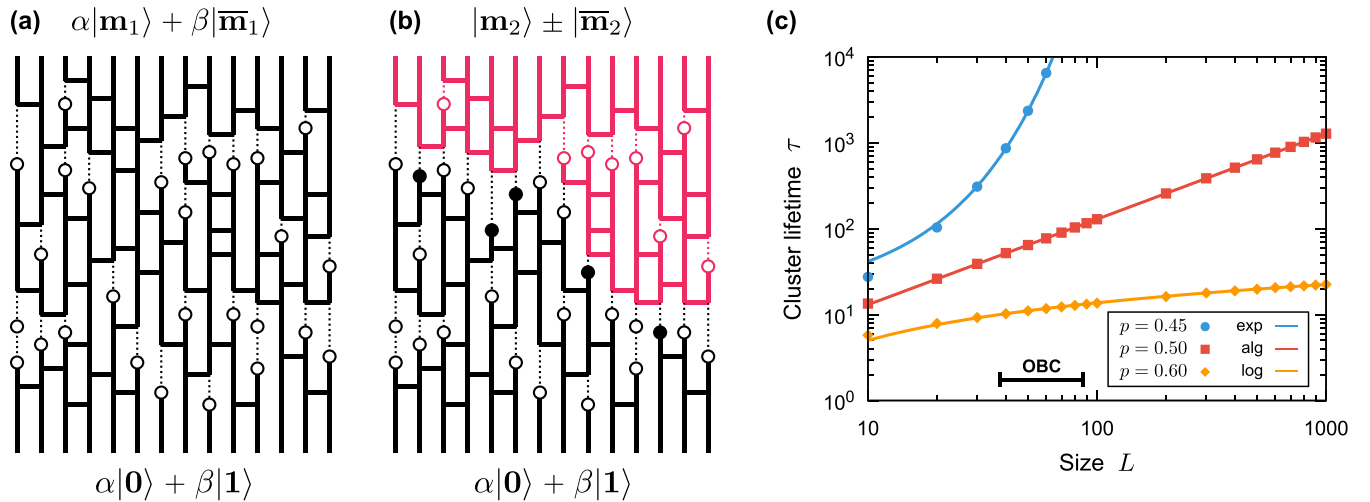


FIG. 8. Quantum error correction. (a),(b) Time evolution with random stabilizer measurements S_e between adjacent qubits (horizontal bars) and random errors E_i on qubits (circles); time runs upwards. The system is initialized in the code space with a global Bell cluster (bold black vertical lines). (a) The initial cluster survives and the amplitudes are preserved. (b) Adding a few additional errors (black disks) makes the black cluster die out, losing all information about the encoded qubit. The new, independent cluster (red) is trivial and does not carry quantum information. (c) Average cluster lifetime τ of a global Bell cluster as function of system size L for $p \in \{0.45, 0.50, 0.60\}$. For $p = 0.45 < p_c$, τ grows exponentially so that the amplitudes of the initial cluster are retained almost indefinitely. At criticality $p = 0.5 = p_c$, τ grows algebraically with $\tau \sim L^\beta$ and $\beta \approx 1$. For $p = 0.6 > p_c$, the growth is only logarithmic. The solid lines are fits of the form $\alpha e^{\beta L}$ (blue), $\alpha L^\beta + \gamma$ (red), and $\alpha \log(L) + \beta$ (yellow). Each point is based on 10^5 sampled trajectories on a chain with open boundary conditions and a cutoff simulation time $t_{\max} = 5 \times 10^4$.

To reveal the connection to the PTIM, we need a spin-1/2 representation of the fermion operators. We opt for the slightly unconventional Jordan-Wigner transformation

$$\gamma_{2i-1} = \prod_{j<i} \sigma_j^x \cdot \sigma_i^z, \quad \gamma_{2i} = \prod_{j<i} \sigma_j^x \cdot \sigma_i^y, \quad (30)$$

which leads to the spin-1/2 representations

$$S_e = \sigma_i^z \sigma_{i+1}^z, \quad E_i = \sigma_i^x. \quad (31)$$

An appropriate basis of the code space is then simply $|g_n\rangle = |n \dots n\rangle$ with $\sigma_i^z \sigma_{i+1}^z |g_n\rangle = |g_n\rangle$ and $n = 0, 1$. In this representation, the qubit is encoded as a global Bell cluster

$$|\Phi\rangle = \alpha|0 \dots 0\rangle + \beta|1 \dots 1\rangle, \quad (32)$$

the random errors E_i correspond to measurements of σ_i^x , and the random measurements of stabilizers S_e to measurements of $\sigma_i^z \sigma_{i+1}^z$. We end up with a new interpretation of the PTIM with open boundaries in one dimension, describing the competition between errors and stabilizer measurements on a Majorana chain quantum code. This representation has also been studied recently as an approximation for the diffusion of Majorana defects [28].

In our previous studies of the PTIM, we initialized the system in the unentangled product state $|\Psi(0)\rangle = |+\dots+\rangle$ and used the PTIM to build up entanglement. Our discussion of the Majorana chain quantum code suggests as initial state the global Bell cluster (32). How long does the system retain information about this qubit in the presence of projective errors and random stabilizer measurements? In our analysis of the PTIM dynamics, we found that the amplitudes α and β survive the merging, growth, and shrinking of clusters. Therefore, the quantum information disappears irretrievably only if the initial cluster is completely degraded. In Fig. 8 we

sketch two quantum trajectories: one where the initial cluster survives (a) and one where it decays (b). For each quantum trajectory $|\Phi(t)\rangle$ with $|\Phi(0)\rangle = |\Phi\rangle$, we can define the time τ_Φ at which the initial cluster dies out. We then define the average cluster lifetime τ by averaging τ_Φ over many quantum trajectories. This time scale defines the characteristic decay time of the stored quantum information in the system.

In Fig. 8(c) we plot the scaling of this time scale τ with the system size L for different probabilities p . Again, the entanglement transition is clearly visible at the critical value $p_c = 0.5$: for $p < p_c$, we find an exponentially diverging lifetime for increasing L , indicating that quantum information can be robustly stored in large systems. By contrast, numerics suggest that the growth of τ is only logarithmic for $p > p_c$, while at criticality $p = p_c$ we find an algebraic behavior $\tau \sim L^\beta$ with $\beta \approx 1$. This observation relates the entanglement transition to the capability of certain topological quantum memories to protect quantum information from decoherence. More specifically, it provides an upper bound for the Majorana chain quantum code with faulty stabilizer measurements, above which the retrieval of quantum information is rendered impossible. This relates to earlier findings by Aharonov [55] who identified a percolation-driven upper bound in generic, noisy quantum circuits above which entanglement is necessarily short-ranged and scalable quantum computation becomes impossible.

We now discuss the typical quantum trajectories in the two regimes in detail. If we start with the initial state $|\Phi\rangle = \alpha|0\rangle + \beta|1\rangle$, let the system evolve under conditions such that the initial cluster survives [as in Fig. 8(a)], and finally measure the stabilizers on all edges, the system ends up in the state $|\Phi'\rangle = \alpha|m\rangle + \beta|\bar{m}\rangle$ where again $|\bar{m}\rangle = \mathcal{U}|m\rangle$ with $\mathcal{U} = \prod_i \sigma_i^x$. Note that, along the time evolution, the sign between

the two amplitudes of the initial cluster may change. However, the last stabilizer measurements that condense all clusters into one always reproduce the correct sign between the amplitudes [to see this, use Eqs. (7)–(10) and generalizations thereof]. The final spin configuration \mathbf{m} in $|\Phi'\rangle$ depends on the measurement outcomes during the evolution and is only known if all measurements are recorded. This implies that the quantum information is still stored in the system—but to *access* the qubit (mandatory for a useful quantum memory), one has to deduce the configuration \mathbf{m} from the collected syndrome measurements in an efficient way. This decoding of the quantum memory (and its efficiency) is beyond the scope of this paper.

Conversely, for quantum trajectories where the initial cluster dies out and the quantum information is lost [as in Fig. 8(b)], the final state is $|\mathbf{m}\rangle + |\bar{\mathbf{m}}\rangle$ with probability $|\alpha + \beta|^2/2$ and $|\mathbf{m}\rangle - |\bar{\mathbf{m}}\rangle$ with probability $|\alpha - \beta|^2/2$. Indeed, the error measurement σ_i^x that eventually removes the initial cluster determines the sign and performs a “measurement” of the observable \mathcal{U} on the stored qubit, projecting the system either into the symmetric or the antisymmetric eigenspace of the symmetry \mathcal{U} .

IX. SUMMARY AND OUTLOOK

In this paper, we introduced and studied the projective transverse field Ising model, a random circuit model where in each time step the noncommuting observables σ_i^x and $\sigma_i^z \sigma_{i+1}^z$ are measured randomly with probabilities p and $1 - p$ on sites and edges, respectively. When averaged over many quantum trajectories, the mutual information between far apart spins behaves like a correlation function in conventional second-order quantum phase transitions: while zero above a critical point p_c , it is finite for $p < p_c$. This emergence of long-range entanglement between spins is only visible in averages over quantum trajectories and not in the (up to symmetries, maximally mixed) density matrix of the system. Using a classical model for the entanglement dynamics—the colored cluster model—we performed extensive numerical simulations and presented an intuitive picture of the entanglement transition which can be understood as the condensation of colored clusters.

We would like to point out that this entanglement transition is not necessarily linked to conventional phase transitions of nonequilibrium steady states in driven dissipative systems [22,23]. Indeed, if one generalizes the projective transverse field Ising model to higher dimensions and adds feedback to the process (say, spin flips that are conditioned on the measurement outcomes), then long-range spin correlations are possible and spontaneous symmetry breaking can occur in the steady state. Such nonequilibrium phase transitions are reflected in the density matrix and seem to be unrelated to the entanglement transition studied in this paper. For instance, in one dimension, no long-range order is possible—but the entanglement transition is still visible in ensembles of quantum trajectories. In higher dimensions, both long-range order and the entanglement transition can be observed; however, the critical points of these transitions are not necessarily the same.

In a next step, we related the projective transverse field Ising model to bond percolation on the space-time lattice of the process. This allowed us to infer the critical point of

the one-dimensional system exactly; we verified this relation also for various lattices in two dimensions. Switching to the continuum paved then the way for a conformal field theory of the critical one-dimensional system. With this machinery, we derived the universal prefactor $\tilde{c} = 3\sqrt{3} \ln(2)/(2\pi)$ that describes the scaling of the entanglement entropy, and the critical exponent $\kappa = 2/3$ that determines the algebraic decay of the mutual information. We compared these results with numerical simulations and found almost perfect agreement with the scaling behavior predicted by conformal field theory.

We concluded the paper with a discussion of the relevance of the entanglement transition to quantum error correction by mapping the system to the Majorana chain quantum code. In this context, the competing random measurements could be identified as random stabilizer measurements and projective errors of the environment. Contrary to typical scenarios, the outcomes of the syndrome measurements were not employed for active error correction as our original model did not include any kind of feedback. Despite this unconventional setting, we showed that there is a hidden transition, parametrized by the relative strength of stabilizer measurements and projective errors, that separates two regimes: in one, the encoded amplitudes are quickly lost irretrievably, whereas in the other, the lifetime of the amplitudes grows exponentially with the system size. It is unclear whether this transition is always identical to the well-known decoding thresholds of active quantum error correction.

ACKNOWLEDGMENTS

We thank M. P. A. Fisher for insightful discussions on entanglement transitions and M. Ammon for discussions on aspects of conformal field theories. This research has received funding from the European Research Council (ERC) under the European Union’s Horizon 2020 research and innovation programme (Grant agreement No. 681208). H.P.B. thanks the KITP for hospitality. This research was also supported by the National Science Foundation under Grant No. NSF PHY-1748958.

APPENDIX: NOTE ON ENTANGLEMENT TRANSITIONS

The entanglement transitions found in random quantum circuits (and the one studied in this work) are characterized by the entanglement of *pure states* (quantified by entanglement entropy or mutual information) when averaged over many independent quantum trajectories. For a single quantum trajectory $|\Psi(t)\rangle$, the entanglement entropy of a subsystem A (at some fixed time) can be deduced from the density matrix $\rho_A = \text{Tr}_{\bar{A}} [|\Psi\rangle\langle\Psi|]$ which, in turn, is completely determined by the expectation values of observables on A . In an experiment, determining expectation values requires many copies of the same pure state to average measurement outcomes. If the state in question *could* be prepared deterministically, this would only pose a technical but not a fundamental problem. However, in the present context, the states of quantum trajectories are prepared randomly with two sources of randomness. First, entangling unitaries and projective measurements are *chosen* randomly according to some predefined distribution. As this randomness is of classical origin (and therefore under

the experimenter's control) it does *not* preclude the deterministic preparation of many copies of the same quantum trajectory. However, the second source of randomness is due to the random *outcomes* of the projective measurements and therefore intrinsically quantum. As we cannot apply projections deterministically, this makes the preparation of many copies of a given quantum trajectory exponentially unlikely and renders the experimental observation of such transitions elusive.

Mathematically, this issue can be traced back to the nonlinear dependence of the entanglement entropy on expectation values of observables. To see this, consider a quantity \mathcal{X} that *can* be written as a linear combination of expectation values, $\mathcal{X}(|\Psi\rangle) = \sum_i \lambda_i \langle \mathcal{O}_i \rangle$; then $\mathcal{O}_{\mathcal{X}} \equiv \sum_i \lambda_i \mathcal{O}_i$ is itself an

observable such that $\mathcal{X}(|\Psi\rangle) = \langle \mathcal{O}_{\mathcal{X}} \rangle$. We are interested in the average of this quantity over many (say M) quantum trajectories $\mathcal{N} = \{|\Psi(\bullet)\rangle\}$ [recall Eq. (6)] which—due to the assumed linearity—can be written as $X = \text{Tr}[\rho \mathcal{O}_{\mathcal{X}}]$ with density matrix

$$\rho \equiv \frac{1}{M} \sum_{|\Psi\rangle \in \mathcal{N}} |\Psi\rangle \langle \Psi|.$$

This quantity is experimentally accessible without any post-selection as it is merely an average of the observable $\mathcal{O}_{\mathcal{X}}$ over the ensemble ρ of quantum trajectories. Unfortunately, the entanglement entropy depends *nonlinearly* on expectation values so that this argument breaks down.

-
- [1] J. Eisert, M. Cramer, and M. B. Plenio, Colloquium: Area laws for the entanglement entropy, *Rev. Mod. Phys.* **82**, 277 (2010).
- [2] M. Levin and X.-G. Wen, Detecting Topological Order in a Ground State Wave Function, *Phys. Rev. Lett.* **96**, 110405 (2006).
- [3] A. Kitaev and J. Preskill, Topological Entanglement Entropy, *Phys. Rev. Lett.* **96**, 110404 (2006).
- [4] D. A. Abanin, E. Altman, I. Bloch, and M. Serbyn, Colloquium: Many-body localization, thermalization, and entanglement, *Rev. Mod. Phys.* **91**, 021001 (2019).
- [5] Y. Li, X. Chen, and M. P. A. Fisher, Quantum Zeno effect and the many-body entanglement transition, *Phys. Rev. B* **98**, 205136 (2018).
- [6] A. Chan, R. M. Nandkishore, M. Pretko, and G. Smith, Unitary-projective entanglement dynamics, *Phys. Rev. B* **99**, 224307 (2019).
- [7] B. Skinner, J. Ruhman, and A. Nahum, Measurement-Induced Phase Transitions in the Dynamics of Entanglement, *Phys. Rev. X* **9**, 031009 (2019).
- [8] Y. Li, X. Chen, and M. P. A. Fisher, Measurement-driven entanglement transition in hybrid quantum circuits, *Phys. Rev. B* **100**, 134306 (2019).
- [9] Y. Bao, S. Choi, and E. Altman, Theory of the phase transition in random unitary circuits with measurements, *Phys. Rev. B* **101**, 104301 (2020).
- [10] A. Nahum, J. Ruhman, S. Vijay, and J. Haah, Quantum Entanglement Growth Under Random Unitary Dynamics, *Phys. Rev. X* **7**, 031016 (2017).
- [11] C. W. von Keyserlingk, T. Rakovszky, F. Pollmann, and S. L. Sondhi, Operator Hydrodynamics, OTOCs, and Entanglement Growth in Systems Without Conservation Laws, *Phys. Rev. X* **8**, 021013 (2018).
- [12] A. Nahum, S. Vijay, and J. Haah, Operator Spreading in Random Unitary Circuits, *Phys. Rev. X* **8**, 021014 (2018).
- [13] Q. Tang and W. Zhu, Measurement-induced phase transition: A case study in the nonintegrable model by density-matrix renormalization group calculations, *Phys. Rev. Research* **2**, 013022 (2020).
- [14] O. Alberton, M. Buchhold, and S. Diehl, Trajectory dependent entanglement transition in a free fermion chain – from extended criticality to area law, [arXiv:2005.09722](https://arxiv.org/abs/2005.09722) [cond-mat.stat-mech].
- [15] D. Gottesman, Class of quantum error-correcting codes saturating the quantum Hamming bound, *Phys. Rev. A* **54**, 1862 (1996).
- [16] D. Gottesman, Stabilizer codes and quantum error correction, [arXiv:quant-ph/9705052](https://arxiv.org/abs/quant-ph/9705052) [quant-ph].
- [17] S. Aaronson and D. Gottesman, Improved simulation of stabilizer circuits, *Phys. Rev. A* **70**, 052328 (2004).
- [18] D. Fattal, T. S. Cubitt, Y. Yamamoto, S. Bravyi, and I. L. Chuang, Entanglement in the stabilizer formalism, [arXiv:quant-ph/0406168](https://arxiv.org/abs/quant-ph/0406168) [quant-ph].
- [19] A. Zabalo, M. J. Gullans, J. H. Wilson, S. Gopalakrishnan, D. A. Huse, and J. H. Pixley, Critical properties of the measurement-induced transition in random quantum circuits, *Phys. Rev. B* **101**, 060301(R) (2020).
- [20] C.-M. Jian, Y.-Z. You, R. Vasseur, and A. W. W. Ludwig, Measurement-induced criticality in random quantum circuits, *Phys. Rev. B* **101**, 104302 (2020).
- [21] Y. Li, X. Chen, A. W. W. Ludwig, and M. P. A. Fisher, Conformal invariance and quantum non-locality in hybrid quantum circuits, [arXiv:2003.12721](https://arxiv.org/abs/2003.12721) [quant-ph].
- [22] S. Diehl, A. Micheli, A. Kantian, B. Kraus, H. P. Büchler, and P. Zoller, Quantum states and phases in driven open quantum systems with cold atoms, *Nat. Phys.* **4**, 878 (2008).
- [23] N. Lang and H. P. Büchler, Exploring quantum phases by driven dissipation, *Phys. Rev. A* **92**, 012128 (2015).
- [24] P. Calabrese and J. Cardy, Entanglement entropy and quantum field theory, *J. Stat. Mech.: Theory Exp.* (2004) P06002.
- [25] P. Calabrese and J. Cardy, Entanglement entropy and conformal field theory, *J. Phys. A: Math. Theor.* **42**, 504005 (2009).
- [26] A. Y. Kitaev, Unpaired Majorana fermions in quantum wires, *Phys. Usp.* **44**, 131 (2001).
- [27] S. Bravyi, B. M. Terhal, and B. Leemhuis, Majorana fermion codes, *New J. Phys.* **12**, 083039 (2010).
- [28] A. Nahum and B. Skinner, Entanglement and dynamics of diffusion-annihilation processes with Majorana defects, *Phys. Rev. Research* **2**, 023288 (2020).
- [29] A. Lavasani, Y. Alavirad, and M. Barkeshli, Measurement-induced topological entanglement transitions in symmetric random quantum circuits, [arXiv:2004.07243](https://arxiv.org/abs/2004.07243) [quant-ph].
- [30] S. Sang and T. H. Hsieh, Measurement protected quantum phases, [arXiv:2004.09509](https://arxiv.org/abs/2004.09509) [cond-mat.stat-mech].

- [31] M. Ippoliti, M. J. Gullans, S. Gopalakrishnan, D. A. Huse, and V. Khemani, Entanglement phase transitions in measurement-only dynamics, [arXiv:2004.09560](https://arxiv.org/abs/2004.09560) [quant-ph].
- [32] H. Casini and M. Huerta, A finite entanglement entropy and the c-theorem, *Phys. Lett. B* **600**, 142 (2004).
- [33] G. D. Chiara and A. Sanpera, Genuine quantum correlations in quantum many-body systems: A review of recent progress, *Rep. Prog. Phys.* **81**, 074002 (2018).
- [34] M. F. Sykes and J. W. Essam, Some Exact Critical Percolation Probabilities for Bond and Site Problems in Two Dimensions, *Phys. Rev. Lett.* **10**, 3 (1963).
- [35] S. C. van der Marck, Percolation thresholds and universal formulas, *Phys. Rev. E* **55**, 1514 (1997).
- [36] S. Redner and H. E. Stanley, Anisotropic bond percolation, *J. Phys. A: Math. Gen.* **12**, 1267 (1979).
- [37] C. Bezuidenhout and G. Grimmett, Exponential decay for subcritical contact and percolation processes, *Ann. Probab.* **19**, 984 (1991).
- [38] G. Grimmett, The random-cluster model, in *Probability on Discrete Structures*, edited by H. Kesten (Springer Berlin Heidelberg, Berlin, Heidelberg, 2004), pp. 73–123.
- [39] G. R. Grimmett, T. J. Osborne, and P. F. Scudo, Entanglement in the quantum Ising model, *J. Stat. Phys.* **131**, 305 (2008).
- [40] G. R. Grimmett, Space-time percolation, in *In and Out of Equilibrium 2*, edited by V. Sidoravicius and M. E. Vares (Birkhäuser Basel, Basel, 2008), pp. 305–320.
- [41] Y. Deng and H. W. J. Blöte, Anisotropic limit of the bond-percolation model and conformal invariance in curved geometries, *Phys. Rev. E* **69**, 066129 (2004).
- [42] R. J. Baxter, S. B. Kelland, and F. Y. Wu, Equivalence of the Potts model or Whitney polynomial with an ice-type model, *J. Phys. A: Math. Gen.* **9**, 397 (1976).
- [43] J. Cardy, Conformal invariance and statistical mechanics, in *Fields, Strings and Critical Phenomena*, Les Houches 1988, Session XLIX, edited by E. Brézin and J. Zinn-Justin (Elsevier Science Ltd., Amsterdam, 1990).
- [44] H. van Beijeren, Exactly Solvable Model for the Roughening Transition of a Crystal Surface, *Phys. Rev. Lett.* **38**, 993 (1977).
- [45] B. Nienhuis, Coulomb gas formulation of two-dimensional phase transitions, in *Phase Transitions and Critical Phenomena*, edited by J. L. Lebowitz and C. Domb (Academic Press, New York, 1987), pp. 1–53.
- [46] H. J. F. Knops, Renormalization connection between the eight-vertex model and the Gaussian model, *Ann. Phys. (NY)* **128**, 448 (1980).
- [47] M. den Nijs, Extended scaling relations for the magnetic critical exponents of the Potts model, *Phys. Rev. B* **27**, 1674 (1983).
- [48] J. Cardy, Conformal field theory and statistical mechanics, in *Exact Methods in Low-dimensional Statistical Physics and Quantum Computing*, Les Houches 2008, Session LXXXIX, edited by V. Pasquier, D. Serban, L. Cugliandolo, J. Jacobsen, and S. Ouvry (Oxford University Press, Oxford, 2010).
- [49] H. W. J. Blöte, J. L. Cardy, and M. P. Nightingale, Conformal Invariance, the Central Charge, and Universal Finite-Size Amplitudes at Criticality, *Phys. Rev. Lett.* **56**, 742 (1986).
- [50] J. L. Jacobsen and H. Saleur, Exact Valence Bond Entanglement Entropy and Probability Distribution in the XXX Spin Chain and the Potts Model, *Phys. Rev. Lett.* **100**, 087205 (2008).
- [51] S. Choi, Y. Bao, X.-L. Qi, and E. Altman, Quantum Error Correction in Scrambling Dynamics and Measurement Induced Phase Transition, *Phys. Rev. Lett.* **125**, 030505 (2020).
- [52] M. J. Gullans and D. A. Huse, Dynamical purification phase transitions induced by quantum measurements, [arXiv:1905.05195](https://arxiv.org/abs/1905.05195) [quant-ph].
- [53] M. J. Gullans and D. A. Huse, Scalable Probes of Measurement-Induced Criticality, *Phys. Rev. Lett.* **125**, 070606 (2020).
- [54] N. Lang and H. P. Büchler, Strictly local one-dimensional topological quantum error correction with symmetry-constrained cellular automata, *SciPost Phys.* **4**, 007 (2018).
- [55] D. Aharonov, Quantum to classical phase transition in noisy quantum computers, *Phys. Rev. A* **62**, 062311 (2000).